KLOE-2 Collaboration - LNF Group

D. Babusci, C. Bloise, F. Bossi, G. Capon (Ass.), E. De Lucia (Resp.), A. De Santis, P. De Simone, D. Domenici,G. Fortugno (Tec.), S. Giovannella, M. Martini (Ass)*, S. Miscetti, P. Santangelo, F. Sborzacchi (Tec.).

Also Dipartimento di Scienze e Tecnologie applicate,"Guglielmo Marconi" University, Rome, Italy

1 Introduction

The largest sample ever collected at the $\phi(1020)$ meson peak at e^+e^- colliders is represented by KLOE and KLOE-2 data set of about 2.4×10^{10} ϕ-meson produced. The focus of the physics program being on K_S and η meson rare decays as well as on kaon interferometry, fundamental symmetry tests and physics beyond the Standard Model and including also searches for new exotic particles that could constitute the dark matter. Activities are mainly focused on data reconstruction and analysis towards precise measurements in both kaon and hadron sectors. A sample of 5.1 fb^{-1} has been reconstructed and 2.5 fb^{-1} MC data sample produced, together with 1 fb^{-1} reconstructed data with ROOT output accoring to the experiment long-term Data Preservation plan, exploiting the features of the experiment CED expanded and renewed for Data Consolidation. Within the Data Preservation plan, the CED almost completed the Data Migration from the old IBM3494 to the new TS4500 tape library together with copy of the almost 50% of the RAW data into the disaster recovery LTO tape library,

KLOE-2 Collaboration submitted to JHEP the paper on precision tests of Quantum Mechanics and CPT symmetry with entangled neutral kaons [1)]. From the fit of the observed Δt distribution, being Δt the difference of the kaon decay times, the decoherence and CPT violation parameters of various phenomenological models are measured with a largely improved accuracy with respect to previous analyses, providing the most stringent limits up to date on the considered models.

Latest physics results achieved in 2021 are: i) the final results on the search for decoherence and CPTV in $\phi \to K_S K_L \to \pi^+\pi^-\pi^+\pi^-$, ii) final results on the direct test of T and CPT symmetries in neutral kaon transitions, iv) the preliminary branching ratio measurement of $\eta \to \pi^0\gamma\gamma$ decay, one of the golden tests of Chiral Perturbation Theory, which agrees with the previous KLOE preliminary result at $1.2\,\sigma$ level, confirming the discrepancy with the Crystal Ball measurement, iii) a clear evidence of π^0 tagged events has been established also with the HET positron station data in the search for candidates of single-π^0 production from $\gamma\gamma$ scattering with 3 fb^{-1} KLOE-2 data, v) the preliminary cross-section measurement for the $\pi^+\pi^-\pi^0$ final state around the ω-meson resonance and vi) the final invariant mass distributions from $\phi \to \eta B \to \eta\pi^0\gamma$ to search for the B-boson, a leptophobic mediator between the dark sector and the Standard Model.

2 Data Reconstruction and MC simulation

The final round of data processing was started in March 2020 with a reconstruction average rate of about 20 pb^{-1}/day and 30 pb^{-1}/day peak rate, similarly to the previous data processing campaign. A total 5.1 fb^{-1} have been reconstructed by January 2022 by means of the improved version of the official reconstruction software, so-called DBV-40.
Concerning the Monte Carlo production, the processing of the data started in September 2021 and has reach a total of 2.5 fb^{-1} data produced with a peak production rate of about 40 pb^{-1}/day. The simulation and reconstruction of the full data set is currently ongoing. According to the KLOE-2 long-term Data Preservation plan, along with the reconstruction of the data and the simulation, a

ROOT output of the reconstructed data is being produced. The ROOT file creation relays on the already reconstructed data with the DBV-40 and is inexpensive in terms of CPU time. So far, a sample of about 1 fb^{-1} is available.

3 CED

During the last year, beside the usual activities, KLOE CED carried on some significant consolidation and preservation tasks, started in 2019 and continued during 2020, together with others related to the system management. *Data Preservation* went ahead intermittently, due to the heavy data reconstruction activity, moving the precious KLOE and KLOE-2 raw data from both the old IBM3494 and new TS4500 tape libraries to a disaster recovery LTO tape library.

More than 95% of the whole data-set has been copied, while the reconstruction was going on, from the old 3494 tape library and 50% of the raw data has been copied into LTO tape. The data preservation task will require several months in 2022 to be accomplished.

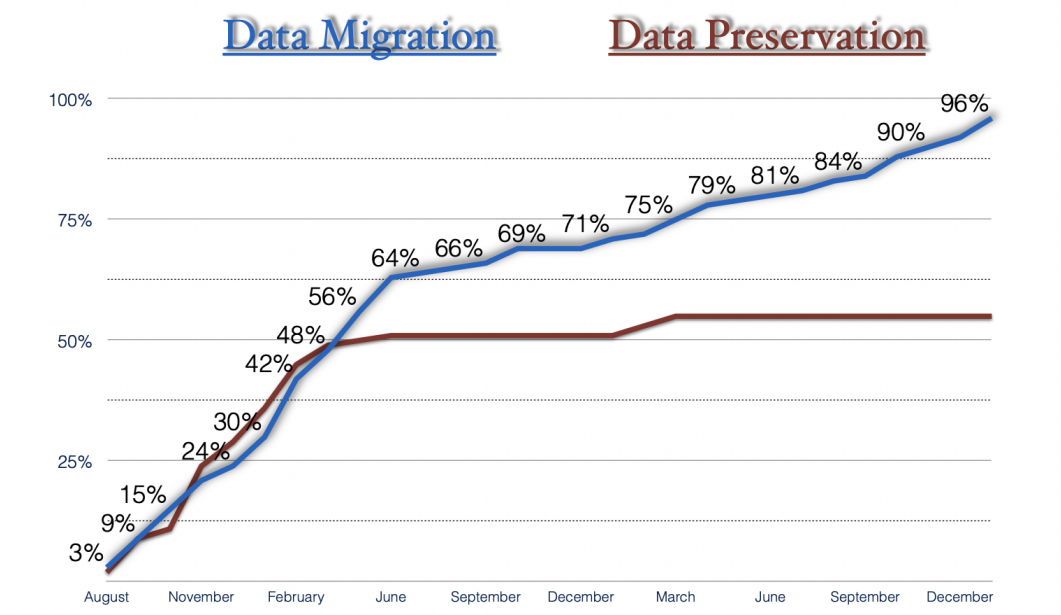

Figure 1: KLOE CED Data consolidation and Data preservation rate

The disk infrastructure became faster, managed with the GPFS protocol, with two different disk arrays controlled by IA. Both arrays achieve the wonderful rank of 8 Gigabyte per second of total throughput. The throughput is very high also when our cluster is working at full rank, with 800 different reconstruction jobs which make IO activities up to 20000 files at the same time. This result has been reached and fixed with software and hardware both focused to keep the speed in every working condition. Fig.2 The redundant Storage Area Network with fibre channel protocol and the GPFS protocol managing the disk array controlled by IA, caching system with hierarchical device tiering, make the infrastructure so strong to work for many weeks without interruption and without slowing down the efficiency or decreasing the throughput level.
The new job submission system based upon GPFS file system, which replaced the old one compatible with AFS file systems, managed more than 100.000 jobs during the last year without missing

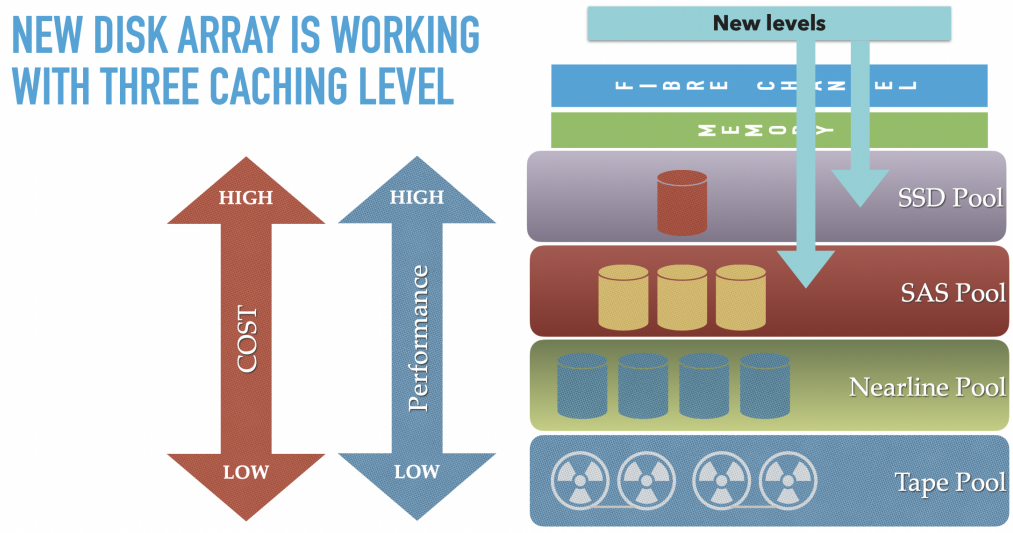

Figure 2: New Disk Arrays hierarchical access method.

even a single job. It dispatched and managed more efficiently the load into the KLOE computing cluster, working as a High Performance Computing in parallel way with a high level of latency. This cluster with the new job submission system is the keystone of the KLOE tasks, fitting the jobs to the cluster resources without making over heading even a single processor, so to keep the efficiency at the top level. The analysis, the reconstruction and the Monte Carlo production are now managed by the submission system with different priority, altered every time the KLOE policy board changed the priority of the different tasks involved.
The structure of KLOE CED has become more compact and efficient, reliable and reactive to the user's requests with the GPFS as a new data distribution centre. Every client has a multi-path channel to read and write data guaranteed as speed, to reduce the wait time for every IO operation. The increase in terms of speed is the cornerstone of the new architecture, started in 2019 and completed during the 2020.

This consolidated architecture with the storage area network, allows for every task, to reach the best level of efficiency and beside has deployed a new data redundant distribution system. This redundant architecture led to zero the number of jobs slowed down due to the disks I/O congestion.

The AI and the SDD disk tearing level, deploy at the highest access performance for writing programs.

Night and day, there is an AI working to organise and optimise the access to the files belong to the array. The IA is moving files in and out from the three caching levels with the purpose to minimise the access time and as shown in the Fig.3, the result are outstanding. Every time the AI model controlling the file distribution is becoming more expert of our file usage and the files necessary to jobs running into the HPC cluster are managing to increase the speed and lower the access time. Now, every job running on the cluster works without interference from other jobs, it works like if it was alone into the cluster. The algorithm of the AI designed to satisfy the file hungry jobs have suited to our typical job request and is becoming every day better in its tasks. The other improvement of our CED along the year, has been on the Storage Area Network. We changed two old switch CISCO with new ones and we moved from 16 Gbit interfaces to 32 Gbit new interfaces. This increases the total throughput by a factor 4. The new CISCO fibre channel switches allow the

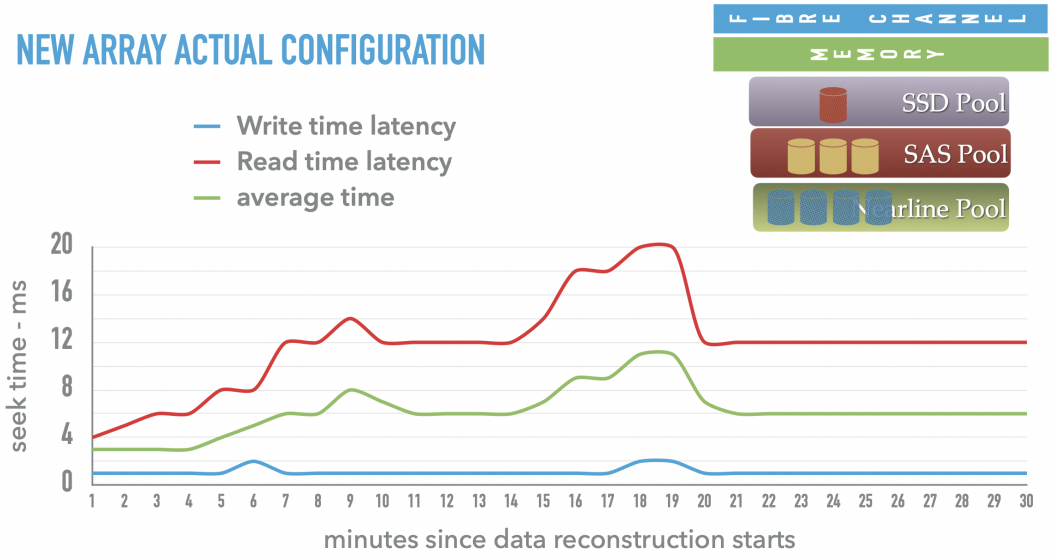

Figure 3: Disk Arrays read and write latency.

tape interfaces and the disk array interfaces to work at full speed. Because the port interfaces of the tape drive or the disk arrays cannot be increased by number, reaching the full speed is a good enhancement for our storage network. We can also increase, in this way, the maximum number of files exchanged from programs to devices or from device to device. Now in a normal run with HPC cluster, the storage area network can manage more than 40000 file simultaneously without delays due to IO wait times. Our Storage Network can face challenging tasks like physics modelling or parallel fluid-dynamics programs which represent the highest difficult programs level into the whole programming world. The environment required to run those programs is now available into our cluster. The CPU and the infrastructure are able to run those programs which are the most difficult programs of the computing world to run. So, we managed the tasks required from KLOE-2 experiment reconstruction and analysis in a powerful environment act to solve every request needed. Continuous studies for a new computational models has been developed with the not used power or during the idle time of the main tasks, because every simulation runs in a parallel environment extruded from the main one, partitioning resources and using them to bump not into one another.

4 Physics achievements

In the following sections latest achievements obtained analysing the unique data sample collected by KLOE and KLOE-2 experiments will be discussed, in both kaon and hadron sectors. The results were also shown at several conferences among which EPS-HEP 2021, Hadron 2021 and Panic 2021.

4.1 Search for decoherence and CPT violation in $\phi \to K_S K_L \to \pi^+\pi^-\pi^+\pi^-$

The quantum interference between the decays of entangled neutral kaons is studied in the process $\phi \to K_S K_L \to \pi^+\pi^-\pi^+\pi^-$, which exhibits the characteristic Einstein–Podolsky–Rosen correlations that prevent both kaons to decay into $\pi^+\pi^-$ at the same time. This represents a very powerful tool allowing the quantum coherence of the entangled kaon pair state to be tested at

the utmost precision, and to search for minute decoherence and violation effects, which may be justified in a quantum gravity framework.

The analysed data sample is about 1.7 fb^{-1} corresponding to $\sim 1.7 \times 10^9$ $\phi \to K_S K_L$ decays. According to the ϕ-meson quantum numbers, the produced neutral kaon system has to be fully antisymmetric implying a complete cancellation of the combined decay amplitudes in the same final state for the two kaons. By considering the decay amplitude as a function of the decay time difference for the two kaons in the $\pi^+\pi^-$ final state, a fully destructive interference is expected, and indeed observed, for equal decay time (Fig. 4 left).

Assuming a violation of the standard quantum-mechanical time evolution of the system, it is possible to introduce a fully phenomenological approach by inserting an extra parameter accounting for the deviation from the expected behavior. This term, known a "decoherence" parameter, appears in the amplitude equation with the neutral kaon state projected alongside the flavor eigenstate [2]:

$$I(\pi^+\pi^-,\pi^+\pi^-;\Delta t) = \frac{N}{2}\Big[\big|\langle\pi^+\pi^-,\pi^+\pi^-|K^0\bar{K}^0(\Delta t)\rangle\big|^2 + \big|\langle\pi^+\pi^-,\pi^+\pi^-|\bar{K}^0K^0(\Delta t)\rangle\big|^2 \qquad (1)$$

$$-2(1-\zeta_{00})\Re e(\langle\pi^+\pi^-,\pi^+\pi^-|K^0\bar{K}^0(\Delta t)\rangle\langle\pi^+\pi^-,\pi^+\pi^-|K^0\bar{K}^0(\Delta t)\rangle^*)\Big]$$

The decoherence parameter can be introduced also using the mass eingestate representation (ζ_{SL}). Other mechanisms could be assumed, among these are the ones relating the decoherence of the system time evolution to CPT violation through quantum gravity effects. In this case other parameters are introduced to describe the modified evolution time of the entangled kaon system (γ) [3] or the modification of the initial state ($|\omega|e^{i\phi_\omega}$) [4]. From the fit of the observed Δt distribution

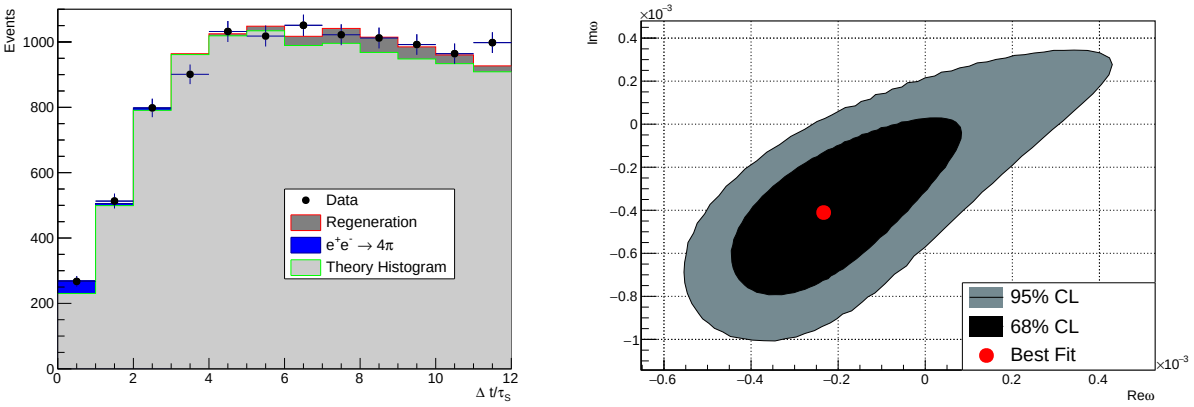

Figure 4: Left: distribution of the time difference between same decay ($\pi^+\pi^-$) of the two kaons. The Data distribution (dots) is compared with theoretical prediction from the fit for the ζ_{SL} decoherence model with background contributions displayed (shaded histograms). The effect of resolution on the reconstruction of the decay vertices can be appreciated in the first bins, where the effect of the quantum correlation causes a complete drop to zero of the theoretical distribution. Right: ω model contour plot for the 68% and 95% confidence levels

(Fig. 4 left), with Δt being the difference of the kaon decay times, the decoherence and CPT violation parameters of various phenomenological models have been measured with a largely improved accuracy with respect to previous analyses, providing the most stringent limits up to date on the

considered models. The final results for the decoherence parameters $\zeta_{\rm SL}$, $\zeta_{00\bar{0}}$, and γ are [1]:

$$\zeta_{\rm SL} = (0.1 \pm 1.6_{\rm stat} \pm 0.7_{\rm syst}) \cdot 10^{-2} \text{ with } \chi^2/\text{dof} = 11.2/10 \ ,$$
$$\zeta_{00\bar{0}} = (-0.05 \pm 0.80_{\rm stat} \pm 0.37_{\rm syst}) \cdot 10^{-6} \text{ with } \chi^2/\text{dof} = 11.2/10 \ ,$$
$$\gamma = (0.13 \pm 0.94_{\rm stat} \pm 0.42_{\rm syst}) \cdot 10^{-21} \text{ GeV with } \chi^2/\text{dof} = 11.2/10 \ .$$

together with the results on the complex ω parameter:

$$|\omega| = (4.7 \pm 2.9_{\rm stat} \pm 1.0_{\rm syst}) \cdot 10^{-4},$$
$$\phi_\omega = -2.1 \pm 0.2_{\rm stat} \pm 0.1_{\rm syst} \text{ (rad)} \ \text{ with } \chi^2/\text{dof} = 9.2/9 \ .$$

with Fig. 4 right showing the ω model contour plot for the 68% and 95% confidence levels.

These results are consistent with no deviation from quantum mechanics and CPT symmetry though for some parameters the precision reaches the interesting level at which – in the most optimistic scenarios – quantum gravity effects might show up. The reported results provide the most stringent limits up to date on the considered models.

4.2 Direct test of T and CPT symmetries in neutral kaon transitions

The comparison of neutral meson transition rates between flavour and CP eigenstates allows direct and model independent tests of time-reversal T and CPT symmetries [5] to be performed. To identify the initial state of a particle transition by the decay of its entangled partner quantum entangled kaon pairs are used. The final state instead is tagged by semileptonic and hadronic decays into two and three pions.

T-violation can be tested through the following ratios of the rates of two classes of processes identified in the dataset $K_S K_L \to \pi^\pm e^\mp \nu, 3\pi^0$ and $K_S K_L \to \pi^+\pi^-, \pi^\pm e^\mp \nu$:

$$\mathrm{R}_2(\Delta t) = \frac{\mathrm{P}[\mathrm{K}^0(0) \to \mathrm{K}_-(\Delta t)]}{\mathrm{P}[\mathrm{K}_-(0) \to \mathrm{K}^0(\Delta t)]} \sim \frac{\mathrm{I}(\pi^+ e^- \bar{\nu}, 3\pi^0; \Delta t)}{\mathrm{I}(\pi^+\pi^-, \pi^- e^+ \nu; \Delta t)}, \tag{2}$$

$$\mathrm{R}_4(\Delta t) = \frac{\mathrm{P}[\bar{\mathrm{K}}^0(0) \to \mathrm{K}_-(\Delta t)]}{\mathrm{P}[\mathrm{K}_-(0) \to \bar{\mathrm{K}}^0(\Delta t)]} \sim \frac{\mathrm{I}(\pi^- e^+ \nu, 3\pi^0; \Delta t)}{\mathrm{I}(\pi^+\pi^-, \pi^+ e^- \bar{\nu}; \Delta t)}, \tag{3}$$

with $\mathrm{I}(f_1,f_2;\Delta t)$ denoting the number of recorded events characterized by a time-ordered pair of kaon decays f_1 and f_2 separated by an interval of proper kaon decay times Δt [5]. A deviation from unity of the asymptotic level of these ratios at large transition time values would be a T-violation manifestation.

CPT symmetry can also be tested and in this case the determination of the asymptotic level of this double ratio is used:

$$\frac{R_2^{CPT}}{R_4^{CPT}} = \frac{\mathrm{P}[\mathrm{K}^0(0) \to \mathrm{K}_-(\Delta t)]/\mathrm{P}[\mathrm{K}_-(0) \to \bar{\mathrm{K}}^0(\Delta t)]}{\mathrm{P}[\bar{\mathrm{K}}^0 \to \mathrm{K}_-(\Delta t)]/\mathrm{P}[\mathrm{K}_-(0) \to \mathrm{K}^0(\Delta t)]} \overset{\Delta t \gg \tau_S}{=} 1 - 8Re(\delta) - 8Re(x_-), \tag{4}$$

with δ and x_- being the parameters violating CPT symmetry in $\mathrm{K}^0\bar{\mathrm{K}}^0$ mixing and the $\Delta S = \Delta Q$ rule, respectively. This double ratio represents a robust CPT-violation sensitive observable [5] which has never been measured to date.

The sample analyzed is 1.7 fb^{-1} KLOE data. Event selection efficiencies were evaluated using Monte Carlo simulations and data/MC corrections based on reference channels where necessary. Rates of the aforementioned two classes of processes, expressed as a function of the difference of proper kaon decay times, were compared to obtain T, CP and CPT- violation sensitive observables.

The time-dependent rates were fit in the asymptotic time difference range ($\Delta t >> \tau S$) with a maximum likelihood fit, yielding the following results:

$$\begin{aligned}
R_2^T &= 0.991 \pm 0.017_{\rm stat} \pm 0.017_{\rm syst} \pm 0.012_{\rm D},\\
R_4^T &= 1.015 \pm 0.018_{\rm stat} \pm 0.018_{\rm syst} \pm 0.012_{\rm D},\\
R_2^{CPT} &= 1.004 \pm 0.017_{\rm stat} \pm 0.017_{\rm syst} \pm 0.012_{\rm D},\\
R_4^{CPT} &= 1.002 \pm 0.017_{\rm stat} \pm 0.018_{\rm syst} \pm 0.012_{\rm D},\\
R_2^{CP} &= 0.992 \pm 0.028_{\rm stat} \pm 0.018_{\rm syst},\\
R_4^{CP} &= 1.00665 \pm 0.00093_{\rm stat} \pm 0.00089_{\rm syst},\\
R_2^T/R_4^T &= 0.979 \pm 0.028_{\rm stat} \pm 0.018_{\rm syst},\\
R_2^{CPT}/R_4^{CPT} &= 1.005 \pm 0.029_{\rm stat} \pm 0.018_{\rm syst}.
\end{aligned}$$

where D denotes the uncertainty on the factor D = $\mathrm{BR}(K_L \to 3\pi^0)\tau_S/\mathrm{BR}(K_S \to \pi^+\pi^-)\tau_L$.

4.3 $\eta \to \pi^0\gamma\gamma$

One of the golden tests of Chiral Perturbation Theory is represented by the $\eta \to \pi^0\gamma\gamma$ decay, which is sensitive, both in the branching ratio (BR) and in the $M_{\gamma\gamma}$ spectrum, to the order p^6 term in the effective Lagrangian. [6, 7] The $4\,\sigma$'s tension between the Crystal Ball measurement [8] and the preliminary KLOE result [9] is under investigation at KLOE-2 with an independent and four times larger data sample, corresponding to 1.7 fb^{-1}.

Preselection cuts select 5 and 7 prompt photon candidates. Energy resolution of all variables are then improved using kinematic fits for both samples. The 5γ's sample is used to extract signal events. The main background contribution from $\eta \to \pi^0\pi^0\pi^0$ with lost or merged photons is reduced using the BDT Multi Variate Analysis method, with cluster shapes as input. Other background contributions are rejected by performing ad-hoc kinematic fits constraining $\pi^0\pi^0$ and $\eta\pi^0$ intermediate states.

The signal and background contributions are then extracted with a fit to the $4\,\gamma$'s invariant mass with Monte Carlo shapes, shown in Fig. 5 left. A very data-MC good agreement is obtained, with clear evidence of the signal. The number of signal events is obtained with 10% statistical error: $\mathrm{N_{sig}} = 1250 \pm 130$.

In order to reduce systematic effects, the number of signal events is normalized to the fully neutral $\eta \to \pi^0\pi^0\pi^0$ sample, whose background is well under control and below 1%. Data-MC comparison of the six-photons invariant mass for the 7 prompt γ's sample, reported in Fig. 5 right, shows a good agreement for the normalization sample, too.

The preliminary measurement of the $\eta \to \pi^0\gamma\gamma$ branching ratio is:

$$\mathrm{BR}(\eta \to \pi^0\gamma\gamma) = (1.21 \pm 0.13_{\rm stat}) \times 10^{-4} \tag{5}$$

This result agrees with the previous KLOE preliminary result at $1.2\,\sigma$ level, confirming the discrepancy with the Crystal Ball measurement. Work on systematics is well advanced, as well as the fit to the $\gamma\gamma$ invariant mass.

4.4 π^0 production from $\gamma\gamma$ scattering

The precision measurement of the $\pi^0 \to \gamma\gamma$ width would give insight into low-energy QCD dynamics. To achieve the $\mathcal{O}(1\%)$ precision needed to test theory predictions, KLOE-2 exploits the π^0 production through $\gamma\gamma$ fusion in the $e^+e^- \to e^+e^-\gamma^*\gamma^* \to e^+e^-\pi^0$ reaction [10]. To reduce the

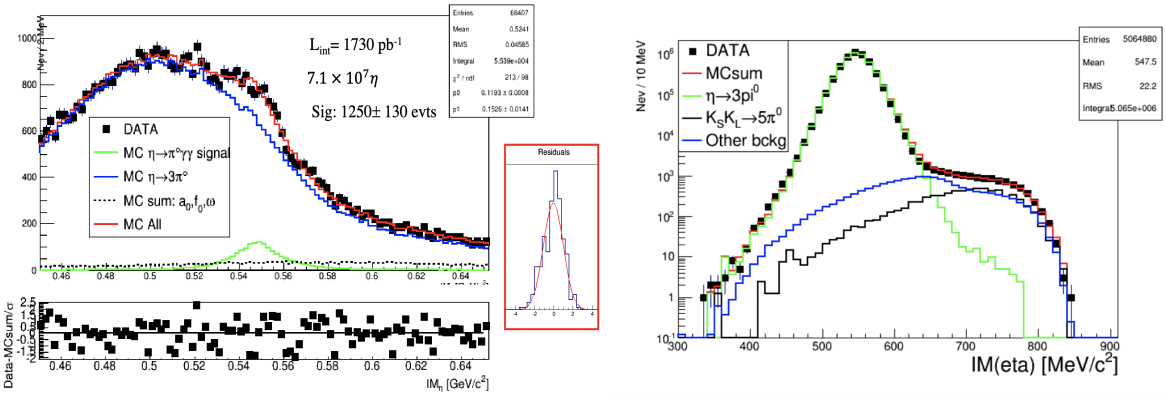

Figure 5: Data-MC comparison for $\eta \to \pi^0\gamma\gamma$ analysis: invariant mass distribution of the four photons assigned to η (left) and of the $\eta \to 3\pi^0$ normalization sample (right). Dots are data, while the different MC contributions are reported as solid lines. For the $4\,\gamma$'s fit, data-MC residuals are also shown.

background from ϕ-meson decays, two High Energy Tagger (HET) stations [11] have been used to detect off-energy leptons scattered in the final state. The HET detectors, made up of 28 plastic scintillators, are installed in roman pots just at the exit of the DAΦNE dipole magnets, 11 m away from the interaction point (IP), both on positron and electron sides. HET scintillators are placed at difference distances from the beam line, scintillators from 1 to 14 are on the horizontal plane of the machine while scintillators from 15 to 28 are displaced by a maximum of 2.8 mm in step on 200 μm, to account for combined effects of the KLOE magnetic field and DAΦNE compensators on the off-energy particles.

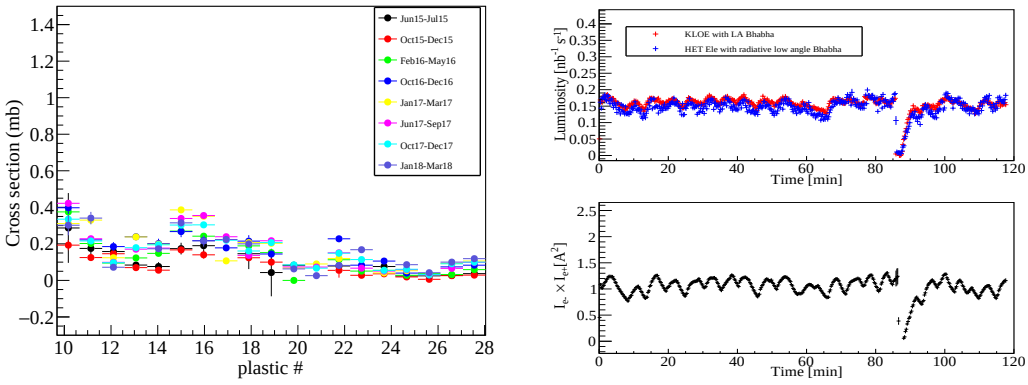

Figure 6: Left panel: effective low-angle radiative Bhabha cross section per plastic as measured by the electron station in the whole data taking period. Top right panel: DAΦNE instantaneous luminosity timeline as measured by the electron station for a single KLOE-2 run acquired in April 2016 (blue); the comparison with the KLOE luminosity measurement is also shown (red). Bottom right panel: timeline of the beam current product for the same run.

The HET acquisition system has been designed to register more than two turns of the machine. Therefore, the time window of the HET data acquisition is wider than KLOE one (~ 250 ns) and

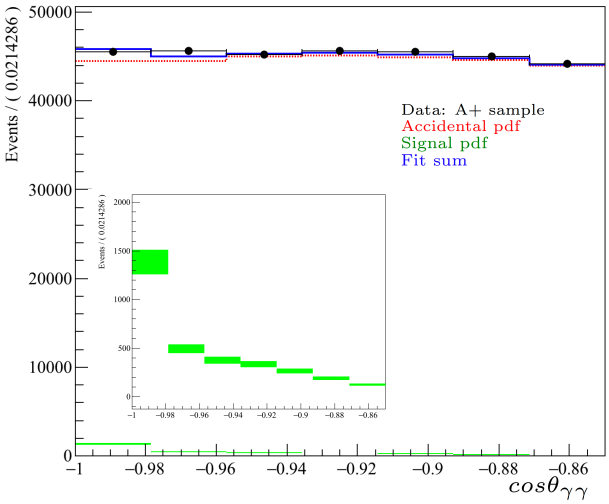

Figure 7: Results of the simultaneous fit of the KLOE-HET coincidence sample (A+), the fit projection on the $cos\theta_{\gamma\gamma}$ variable is shown. Data are the black points, the accidental amount is the red dashed line, the signal is in green while the blue line is the sum of the two fits. Insert is zoom of the signal extracted from the fit.

varies from 660 to 970 ns. $\gamma\gamma \to \pi^0$ signal is expected in the coincidence window between HET and KLOE while the remaining buffer depth, acquired together with the coincidence sample, is used to evaluate the amount of uncorrelated time coincidences between the two detectors (accidentals).

The accidental counting rate is dominated by low-angle radiative Bhabha scattering and we use the effective cross-section, as a function of the data-taking period, to measure the detector acceptance×efficiency and for data quality.

Figure 6 left panel shows the effective low-angle radiative Bhabha cross section per plastic as measured by the electron station in the whole HET data set, for the most stable plastic range 10–28. An effective total average cross section of 2.5 ±0.08 mb has been measured for these plastics with data acquired between 2015 and 2018. The intra-bunch scattering background as function of the data-taking period and per each plastic scintillator has been measured as well, the fraction varies from about 10 to 40% of the total measured HET rate according to the data-taking period. In Figure 6 top right panel, the comparison between the DAΦNE luminosity timeline as measured by the electron station with low angle radiative Bhabha's and KLOE with large angle Bahbah's is shown. As validation, the average effective Bhabha cross section and Touschek fraction, estimated between February and May 2016, have been used to derive the DAΦNE luminosity timeline from the HET electron plastic rates acquired during a single run in April 2016. In the right bottom panel of Figure 6 we report, as reference, the timeline of the product of the beam currents.

For the π^0 search a sub-set of HET plastic scintillators has been used, chosen for their operational stability over time scale of years. Candidates of single-π^0 production from $\gamma\gamma$ scattering have been pre-filtered recording information on the hit in the tagger, on the trigger signal, the DAΦNE operational parameters, clusters and tracks reconstructed in the KLOE central detector. Data are classified as single-arm (SA) or double-arm (DA) events. DA events are selected requiring the time coincidence of the two HET stations within 12 ns, while for SA events, we selected hits in one HET station and at least one bunch in the KLOE central detector associated with only 2 clusters in the calorimeter. Very loose kinematic cuts are applied to this sample. Statistical evidence of correlated coincidence events between the tagger station and the KLOE calorimeter

has been observed on a sample of 3 fb^{-1} (whole reconstructed HET data sample), on the electron side, with a precision of about 10% in a KLOE-HET coincidence window of a few bunches.

Fig. 7 shows the projection, over $cos\theta_{\gamma\gamma}$, of the simultaneous fit on the KLOE-HET coincidence sample (A+ sample) in the $\Delta T_{\gamma\gamma} - \Delta R_{\gamma\gamma}/c$ vs $cos\theta_{\gamma\gamma}$ variables. The A+ sample is constituted by a large amount of accidentals (A sample) and $\gamma\gamma \to \pi^0$ signal. Accidental events coming from ϕ decays and surviving our selections have been totally rejected using information derived from a study performed with GEANFI data. The accidental background is modeled using the HET data acquired out of coincidence window with the KLOE detector, while the $\gamma\gamma \to \pi^0$ signal is taken from the Ekhara simulation [12] interfaced with the BDSIM transport of the leptons through the beam line [13]. A carefully study of the KLOE calorimeter performance and of the KLOE trigger threshold has been performed to properly model the expected $\gamma\gamma \to \pi^0$ signal.

For the first time, a clear evidence of π^0 tagged events has been established also on the HET positron data.

Currently, we are working to: i) improve fit quality and precision on π^0 counting ii) measure the actual HET acceptance ii) extract the preliminary measurement of the $\gamma\gamma \to \pi^0$ cross section.

4.5 $e^+e^- \to \omega\gamma$

The measurement of the hadronic cross section in the low energy mass range (*e.g.* below 1 GeV) can be performed with KLOE-2 data using the so-called ISR technique: the observation of the associated radiative process normalized with the expected differential luminosity. In this analysis this approach is used to observe the for the $\pi^+\pi^-\pi^0$ final state in the mass range around the ω meson resonance, where the cross section can be expressed as:

$$\sigma\left(e^+e^- \to \pi^+\pi^-\pi^0, M_{3\pi}\right) = \frac{\mathrm{d}N_{\mathrm{obs}}(\pi^+\pi^-\pi^0\gamma)/\mathrm{d}M_{3\pi}}{\varepsilon(M_{3\pi})\mathrm{d}L/\mathrm{d}M_{3\pi}} \tag{6}$$

where $M_{3\pi}$ represents the invariant mass of the three pion system, strictly connected to the energy of the radiated photon; ε is the global efficiency (acceptance and selection) as a function of the 3π invariant mass and $\mathrm{d}L/\mathrm{d}M_{3\pi}$ is the differential luminosity at a given 3π invariant mass. The total cross section of the process is described using relativistic Breit-Wigner (BW) formula:

$$\sigma\left(s\right) = 12\pi\mathcal{B}\left(\omega \to e^+e^-\right)\mathcal{B}\left(\omega \to \pi^+\pi^-\pi^0\right)\frac{\Gamma_\omega^2}{\left(s - M_\omega^2\right)^2 + M_\omega^2\Gamma_\omega^2}, \tag{7}$$

The full data-set of KLOE experiment, 1.7 fb^{-1}, has been analyzed looking for the corresponding topology: $\pi^+\pi^-3\gamma$ final state [14]. The event reconstructed information (tracks in the Drift Chamber and clusters in the EM Calorimeter) are processed through global kinematic fit to improve the energy and time determination. The best possible photon pair is used to reconstruct a π^0 candidate, shown in fig.8-(a). Signal kinematic, as obtained from Monte-Carlo simulation, is used to clean the selected sample in order to minimize the background contribution in the event selection.

Monte-Carlo simulated shapes, divided in several different contributions are used to fit the data distribution of the three pions invariant mass, shown in fig.8-(b). Weighting factors determined with the fit procedure are then used to verify the global agreement between data and simulation, before subtracting simulated background event shapes from the data. All comparison between data and simulation reported in the fig.8 uses the weights obtained from the shape fit at the end of the selection chain.

The data distribution, after background subtraction, is show in fig.8-(e), where the preliminary results of the cross section fit are reported. A reasonable agreement between data and

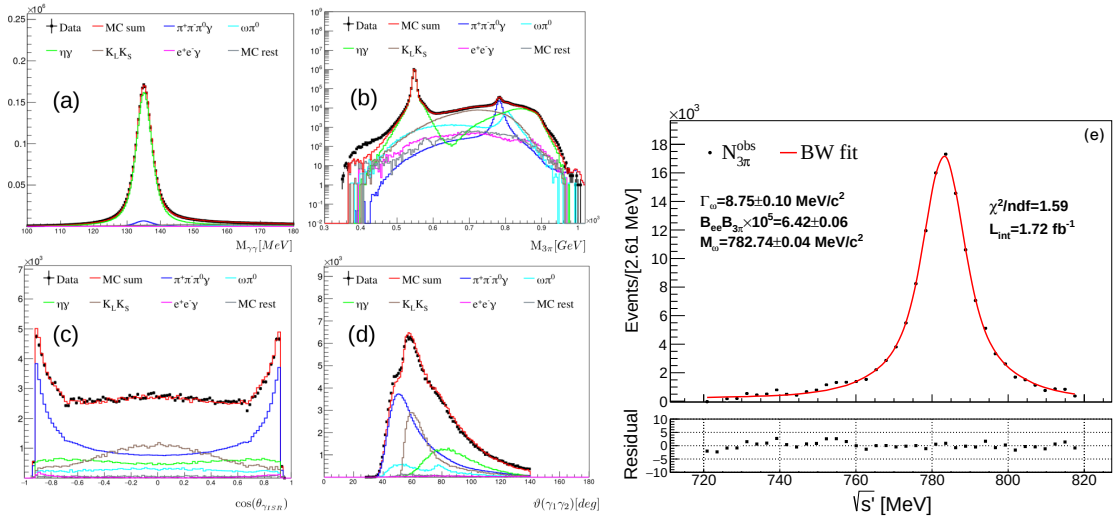

Figure 8: Data-Simulation comparison: $M_{\gamma_1\gamma_2}$, the reconstructed π^0 mass (a); $M_{3\pi}$, the reconstructed omega mass in the whole range (b); $\cos(\theta_{\gamma_{ISR}})$, the polar angle distribution of the radiated photon (c); $\vartheta(\gamma_1\gamma_2)$, the angle between photon associated to the π^0 decay (d). In the plot (e) the invariant mass spectrum is shown after the background subtraction. Data are fitted with a Breit-Wigner distribution to extract ω mass, total width and normalization related to branching fractions products. In the bottom panel the residuals $((N_{Data} - N_{Fit})/\sigma_{Data})$ of the fit as a function of the invariant mass are shown.

Breit-Wigner cross section description is obtained. The evaluation of the systematic uncertainty is still on-going, but preliminary estimates indicates that the contribution should be similar or lower than the statistical contribution.

4.6 Leptophobic Dark Matter search

We conduct the search of a leptophobic mediator between Dark Matter (DM) and SM particles, proposed in [15], using a total of 1.7 fb^{-1} acquired with the KLOE detector The B-boson arises from a new $U(1)_B$ gauge symmetry that couples to the baryon number as:

$$\mathcal{L} = \frac{g_B}{3}\bar{q}\gamma^\mu q B_\mu \tag{8}$$

where g_B is the $U(1)_B$ coupling, estimated to be $g_B \lesssim 10^{-2} \times (m_B/100\ \text{MeV})$. With quantum numbers $I^G(J^{PC}) = 0^-(1^{--})$, the B-boson decays in a similar way as the ω-meson. It is worth noticing that the B-boson cannot be hidden under the ρ meson, given the decay $B \to \pi^+\pi^-$ is forbidden by G-parity.

For masses below 600 MeV, the decay $B \to \pi^0\gamma$ becomes dominant and allows the KLOE detector to search for the B-boson in the 5-γ's final state from the production channel $\phi \to \eta B$. In this case, the B-boson would show as an enhancement in the $\pi^0\gamma$ invariant mass. Fig. 9 left panel shows the $\pi^0\gamma$ invariant mass from the decay $\phi \to \eta B$ with 1.7 fb^{-1} compared to the extracted background using a side-bands fit to the data. Since no signal is found, we proceed to establish a preliminary result on the upper limit as number of excluded events at 90% C.L. for the full mass range, which is presented in Fig. 9 right panel. From this we can expect to set limits in the coupling constant of the B-boson (α_B) at the level of $\mathcal{O}(10^{-7})$ at 90% CLs. The preliminary results were

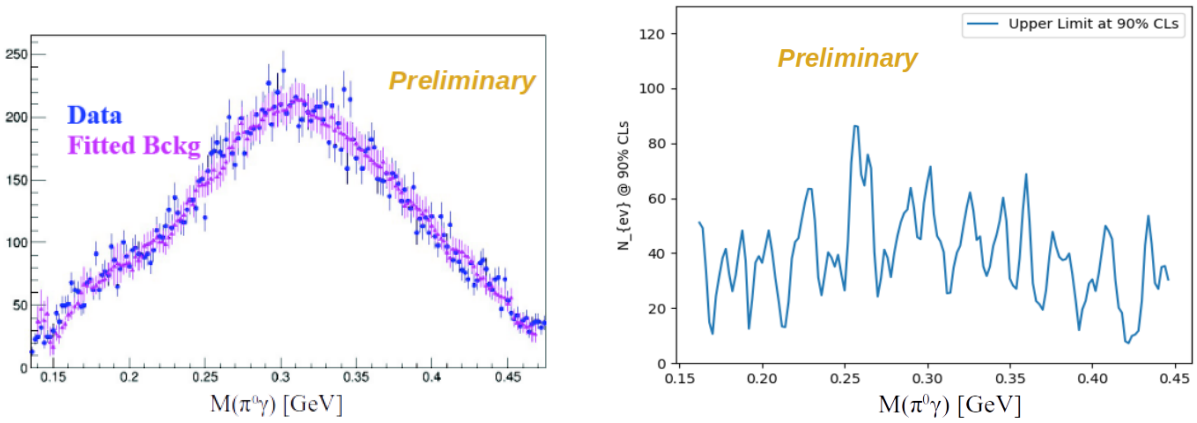

Figure 9: Left panel: Invariant mass of the $\pi^0\gamma$ system from the channel $\phi \to \eta B \to \eta\pi^0\gamma$. Blue solid dots correspond to data, magenta solid triangles are the extrapolated background from the side-bands fit. Right panel: Upper limit in the number of excluded events as a function of the B boson mass at the 90% C.L.

presented at the The 16th International Workshop on Tau Lepton Physics (TAU2021) and The 10th International Workshop on Chiral Dynamics, both hole this year.

References

1. D. Babusci *et al.* [KLOE-2 Collaboration], https://doi.org/10.48550/arXiv.2111.04328 submitted to JHEP
2. R.A. Bertlmann *et al.*Phys. Rev. D 60 (1999)114032; R.A. Bertlmann *et al.* Phys. Rev. A**68** (2003)012111.
3. S. Hawking, Commun. Math. Phys. 87 (1982) 395; J. Ellis *et al.* Nucl. Phys. B**241**(1984) 381; J. Ellis *et al.* Phys. Rev. D**53**(1996)3846.
4. J. Bernabeu *et al.* Phys. Rev. Lett. 92 (2004)131601; J. Bernabeu *et al.* Nucl. Phys. B**744** (2006) 180.
5. Bernabeu, J., Di Domenico, A., Villanueva-Perez, P.: Direct test of time-reversal symmetry in the entangled neutral kaon system at a ϕ-factory. Nucl. Phys. B868, 102–119 (2013). https://doi.org/10.1016/j.nuclphysb.2012.11.009 and Bernabeu, J., Di Domenico, A., Villanueva-Perez, P.: Probing CPT in transitions with entangled neutral kaons. JHEP 10, 139 (2015). https://doi.org/10.1007/JHEP10(2015)139
6. J. Bijnens, Phys. Scripta **T 99** 34 (2002)
7. E. Oset, J. R. Pelaez, L. Roca, Phys. Rev. **D 67** 073013 (2003)
8. B. M. K. Nefkens *et al.*, Phys. Rev. **C 90** 025206 (2014)
9. B. Di Micco *et al.*, Acta Phys. Slov. **56** 403 (2006)
10. D. Babusci et al., Eur. Phys. J. C 72, 1917 (2012)

11. D. Babusci et al., Acta Phys. Pol B 46, 81 (2015)
12. H. Czyz, S. Ivashyn, Comput. Phys. Commun. 182 (2011)
13. I. Agapov, G.A. Blair, S. Malton, L. Deacon, Nucl. Instrum. Meth. A 606, 708 (2009)
14. B. Cao [KLOE-2], PoS **EPS-HEP2021** (2022), 409 doi:10.22323/1.398.0409
15. S. Tulin, Phys. Rev. **D89**, 114008 (2014)